Shape-based and texture-based feature extraction for classification of microcalcifications in mammograms

Hamid Soltanian-Zadeh,[a,b,c] Siamak Pourabdollah-Nezhad,[c,d] Farshid Rafiee-Rad[c,e]

[a]Department of Electrical and Computer Engineering, University of Tehran, Tehran, Iran
[b]Department of Radiology, Henry Ford Health System, Detroit, MI 48202, USA
[c]School of Intelligent Systems, Institute for Studies in Physics and Mathematics, Tehran, Iran
[d]Department of Computer Science, Wayne State University, Detroit, MI, USA
[e]Department of Electrical and Computer Engineering, University of Minnesota, Minneapolis, MN, USA

ABSTRACT

This paper presents and compares two image processing methods for differentiating benign from malignant microcalcifications in mammograms. The gold standard method for differentiating benign from malignant microcalcifications is biopsy, which is invasive. The goal of the proposed methods is to reduce rate of biopsies with negative results. In the first method, we extract 17 shape features from each mammogram. These features are related to shapes of individual microcalcifications or to their clusters. In the second method, we extract 44 texture features from each mammogram using co-occurrence method of Haralick. Next, we select best features from each set using a genetic algorithm, to maximize area under ROC curve. This curve is created using a k-nearest neighbor (kNN) classifier and a malignancy criterion. Finally, we evaluate the methods by comparing ROC's with greatest areas obtained using each method. We applied the proposed methods, with different values of k in kNN classifier, to 74 malignant and 29 benign microcalcification clusters. Truth for each mammogram was established based on the biopsy results. We found greatest area under ROC curve for each set of features used in each method. For shape features this area was 0.82 (k = 7) and for Haralick features it was 0.72 (k = 9).

Keywords: microcalcification, mammogram, feature extraction, texture features, shape features, classification, image processing

1. INTRODUCTION

Screen/film mammography is widely used for early detection of breast cancer, which has been shown to greatly reduce the breast cancer mortality among women.[1] Microcalcifications are tiny deposits of calcium in breast carcinoma. Presence of microcalcification clusters accounts for 30% of abnormality in mammograms. A given cluster of microcalcifications might be associated with a malignant or benign case. Distinguishing between malignant and benign clusters is a difficult and time-consuming task for radiologists. This leads to a high rate of unnecessary biopsies that can be avoided or at least minimized using a computer based classification algorithm. It is of crucial importance to design the classification method in such a way to obtain a high level of true-positive rate while maintaining the false-positive rate at its minimum level. It has been shown that computerized detection and classification methods outperform radiologists' detection and classification.[2]

Microcalcification detection and segmentation is useful for computerized screening of mammomgrams and for classification of malignant and benign clusters.[3] This detection and segmentation has been carried out using mathematical morphology,[4] Karhunen-Loeve (KL) transformation and neural networks,[5] wavelet features,[6] both of wavelet features and gray level statistical features,[7,8] and a multistage scheme consisting of local histogram analysis and a fuzzy rule-based classifier.[9]

One of the most important steps for the classification task is extracting suitable features capable of distinguishing between classes. There have been great efforts spent on extracting appropriate features from microcalcification clusters.[10,11,12,13] Features such as the first-order statistical features based on histogram representing the gray level intensity variation and second-order statistical features based on co-occurrence matrix representing the global textural information have been investigated. Classification of malignant and benign clusters has been done using texture features from spatial gray level dependence (SGLD) matrices[14] in addition to using morphological features[15] and shape features.[12,16] In this paper we propose

and evaluate shape-based and texture-based feature extraction methods for classification of microcalcifications in mammograms.

2. FEATURE EXRACTION METHODS

2.1. Shape Features

The first set of features, proposed for microcalcification classification, is shape features of the microcalcifications and their clusters. The number of features we have extracted in this context is 17. The methods for extracting these features are explained below.

2.1.1. Segmentation of microcalcifications

The first step for extracting the shape features is to separate microcalcifications from the background texture in the mammographic images. We segment the microcalcifictions using a new method, which includes detecting the calcifications with an adaptive filter bank and recovering their shapes with morphological operators. The segmentation process generates an image in which microcalcifications of different sizes are seen with the background texture omitted. We apply this method to all of the clusters and obtain images of the segmented microcalcifications. These images are used in the next steps for extracting the shape features.

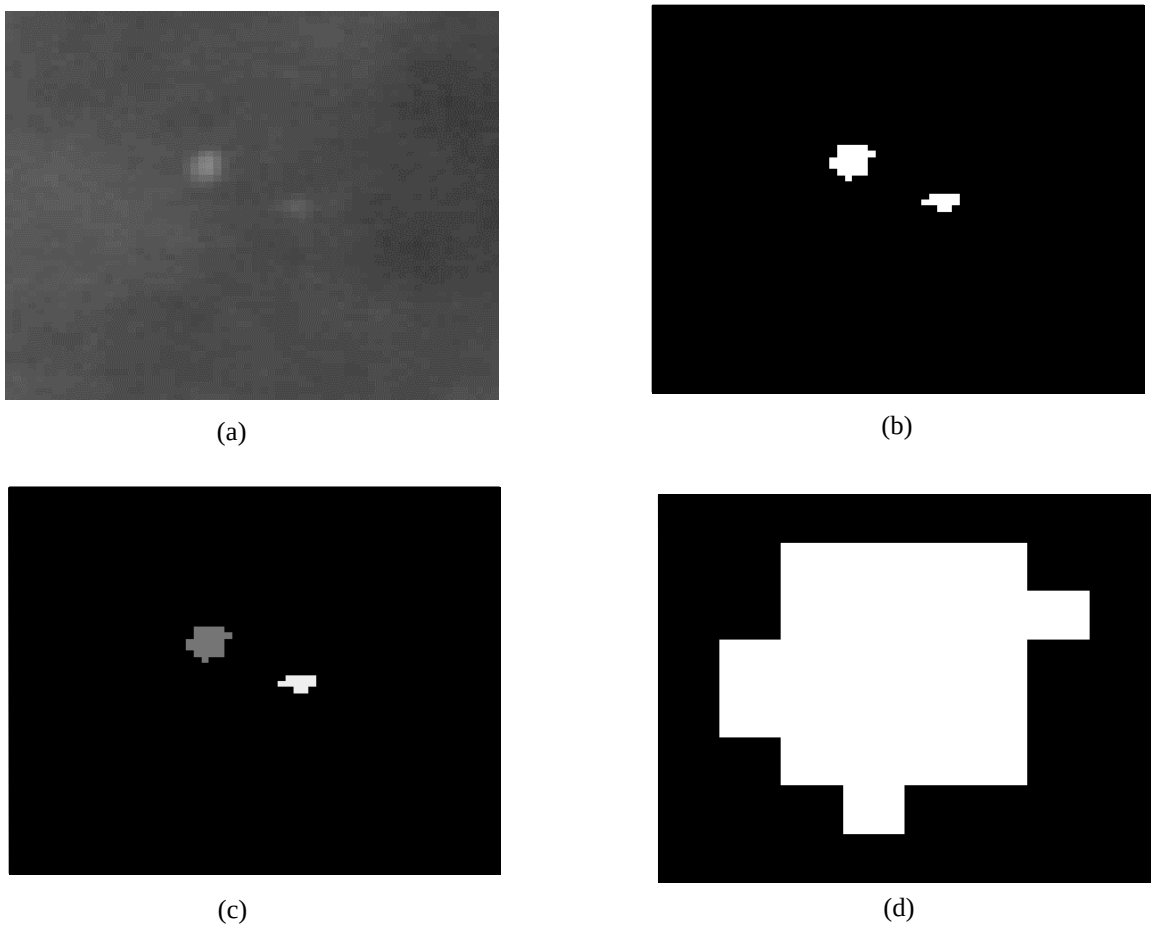

(a) (b) (c) (d)

Fig. 1. (a) A benign microcalcification cluster containing two microcalcifications (b) Segmented microcalcifications (c) Labeled microcalcifications (d) One of the microcalcifications extracted for further processing.

2.1.2. Labeling of microcalcifcations

The next step in our feature extracting procedure is labeling of the separate microcalcifications. This is done for two reasons: determining the number of calcifications in a cluster, and gaining the ability to work with individual microcalcifications. For

this step, the gray-level segmented images, obtained by the above method, are transformed to binary. For extracting features related to the shape of the calcifications, we work on these binary images. The labeling procedure is described below.

Starting from the upper left corner of the image, the labeling pixel *x(i,j)* moves from left to right scanning each row of the image matrix. The first non-zero pixel reached by the labeling pixel is labeled 1. When reaching next pixel, *x(i,j)*, with a value of one (part of a microcalcification), the pixels *x(i,j-1)*, *x(i-1,j)* and *x(i-1,j-1)* are checked out, if they all have a zero value, the label variable is incremented and a new label is assigned to *x(i,j)*, otherwise *x(i,j)* is labeled the same as them. When the labeling pixel reaches the bottom right corner of the image, all of the non-zero pixels in the image have been labeled. If all the islands in the image have a convex shape, the labeling procedure can end here. However, due to the irregular shapes of some of the microcalcifications, parts of some of them might be labeled differently. For overcoming this problem, a new labeling pixel starts moving from the lower right corner of the image and when it reaches a labeled pixel, sets its label to the maximum label value found in the 8 neighboring pixels. This procedure is repeated from the other two corners of the image. Considering all possible shapes for the micrcalcifications, this procedure ensures that all of the pixels belonging to one microcalcification have been labeled the same. Finally, the label numbers are sorted and renamed so that the labels are sequential and in order. The largest label represents the number of microcalcifications in the cluster. In Fig.1(b) the results of applying the segmentation procedure to the microcalcification cluster in Fig.1(a) are shown. The result of the labeling algorithm is shown is Fig.1(c). Fig.1(d) shows a single calcification separated from the cluster for further processing.

2.1.3. Extracting shape features

In this section, we introduce shape features we have extracted for classification of the microcalcification clusters.

2.1.3.1. Features representing size of microcalcifications

One of the characteristics of a microcalcification, which can be a sign of their malignancy, is their sizes. We have used the number of pixels in each mirocalcification as a measure of its size. The corresponding features are: *maximum size of microcalcifications in a cluster*, *standard deviation of size of microcalcifications in a cluster* and *sum of areas of microcalcifications in a cluster*. One form of microcalcifications seen in the mammograms is very small particles with a length less than 100 μm. Their presence can be a sign of malignancy and thus we incorporate *number of microcalcifications with a size of only one pixel* as another feature.

2.1.3.2. Compactness

One of the shape features that has proven to be a good measure for classifying microcalcifications by their shape is compactness.[12] Compactness (C) is defined as the ratio of the squared perimeter (P) to the area (A), i.e.,

$$C = \frac{P^2}{A} \tag{1}$$

Compactness represents the roughness of an object's boundary relative to its area.[12] The smallest value of compactness is 12.56, which is for circle. As circle deviates towards a more complicated shape, compactness becomes larger.

The digital mammograms we have used in this work were scanned with a pixel size of 50 μm and, as mentioned previously, the size of the micrcalcifications might be as small as 100 μm. For such particles, perimeter would have no meaning and it is impossible to calculate compactness for them. Even for larger microcalcifications, the numeric value of compactness would not be accurate. For example, an elongated microcalcification, which is seen as a 2×4 rod would have an area of 8 and a perimeter of the same value and would lead to a compactness of 8, which is theoretically impossible. For eliminating this problem, the first step towards measuring the compactness of the microcalcifications is to upscale them (break each pixel into several smaller pixels). By doing this, the pixels on the contour would occupy a small portion of the area and the calculated value of compactness would be more accurate.

After upscaling the segmented microcalcification clusters, the next step is to separate the isolated calcifications in each cluster, so that the compactness is calculated for each particle. We extract pixels with the same label in each cluster to do this. The next step is marking the contour of each microcalcification. For doing this, we convolve the binary microcalcification image with four filters: $\begin{bmatrix}1 & -1\end{bmatrix}$, $\begin{bmatrix}-1 & 1\end{bmatrix}$, $\begin{bmatrix}-1\\1\end{bmatrix}$, $\begin{bmatrix}1\\-1\end{bmatrix}$ and store the results in four separate matrices. We find the borders by taking the positive values of these matrices and calculating their logical OR.

After calculating the compactness for each of the microcalcifications, the following features are calculated: *maximum value of compactness;* and *average compactness* in each cluster.

2.1.3.3. Moments

Other shape features, which have proved effective for classifying microcalcifications, are moments.[12] The moments we have used are moments of the boundaries. In this definition, boundaries are characterized by an ordered sequence, which represents the Euclidian distances between the centroid of the region and all contour pixels. If $z(i),\ i = 1,\ 2,\ ...,\ N$ are the Euclidian distances of the contour pixels to the centroid (where *N* is the number of these pixels) the *p*th moment is defined as:

$$m_p = \frac{1}{N}\sum_{i=1}^{N}[z(i)]^P \tag{2}$$

And the p*th* central moment is defined as:

$$M_P = \frac{1}{N}\sum_{i=1}^{N}[z(i) - m_1]^P \tag{3}$$

In addition, low-order moment ratios are defined that are less sensitive to noise. These are named as *F1*, *F2*, and *F3*. As examples, *F1* and *F3* are defined below.

$$F1 = \frac{[\frac{1}{N}\sum_{i=1}^{N}[z(i) - m_1]^2]^{\frac{1}{2}}}{\frac{1}{N}\sum_{i=1}^{N}z(i)} \tag{4}$$

$$F3 = \frac{[\frac{1}{N}\sum[z(i) - m_1]^4]^{\frac{1}{4}}}{\frac{1}{N}\sum_{i=1}^{N}z(i)} \tag{5}$$

where

$$m_1 = \frac{1}{N}\sum_{i=1}^{N}[z(i)] \tag{6}$$

It has been shown[12] that *F3-F1* is the best moment feature to represent roughness of microcalcifications. As features for representing the shape of microcalcifications, we have used *maximum value of F3-F1* and *mean of F3-F1* in each cluster. For comparison, we have also taken into account *maximum and mean of F3*.

2.1.3.4. Features related to entire cluster

One important specification, which is considered by radiologists for diagnosing mammograms, is the size of the microcalcification cluster. To represent this parameter, we have used the *radius of the circle that best fits the cluster*, as a feature. Another feature we have extracted for every cluster is the *standard deviation of the distances of the microcalcifications in each cluster to the center of the fitting circle.* This feature would represent the scattering of the microcalcifications, an important factor for classifying them. The *number of microcalcifications in a cluster* is another feature, which is obtained in the labeling procedure.

2.1.4. Extracting other features for appearance of microcalcifications

In addition to the features mentioned above, we have extracted four more features related to the gray levels of the microcalcifications. These features are: *the average gray level for all of the microcalcifications in a cluster, the standard deviation of the mean of the micrcalcification gray levels in a cluster, the maximum standard deviation of the gray levels in each calcification, and the mean standard deviation of the gray levels in each calcification.* In Table I, we have listed the shape features explained above.

Table I. Features related to the shape and appearance of microcalcifications.

1	Number of microcalcifications in the cluster
2	Maximum size of calcifications in the cluster
3	Standard deviation of the size of calcifications in the cluster
4	Number of calcifications with a size of one pixel
5	Sum of the areas of the calcifications in the cluster
6	Maximum value of compactness in the cluster
7	Average compactness in the cluster
8	Maximum value of F3-F1 in the cluster
9	Average F3-F1 in the cluster
10	Maximum value of F3 in the cluster
11	Average F3 in the cluster
12	Radius of the circle that best fits the cluster
13	Scattering of the microcalcifications
14	Average gray level of the microcalcifications in the cluster
15	Standard deviation of the mean of the micrcalcification gray levels in the cluster
16	Maximum standard deviation of the gray levels in each calcification in the cluster
17	Average standard deviation of the gray levels in each calcification in the cluster

2.2. Haralick Features

The second set of features proposed for classification of the microcalcification clusters is the set of features extracted using the co-occurrence matrix. The method we have used for feature extraction is the one proposed by Haralick, namely the spatial gray-level dependence method (SGLDM). The features have previously been used for diagnosis and tracking of Alzheimer's disease in MR images[15, 17] for microcalcification classification in mammography.

In our work, we investigate two approaches for extracting these features. First, we examine the texture of the segmented microcalcifications. Secondly, we examine the texture of the microcalcification clusters including the image's background. For the first approach, we obtain images in which only the calcifications are present. For this reason, we use the segmentation method we introduced in the previous section. Then the segmented binary images are multiplied by the original images from which they were obtained. This procedure generates images containing only the calcifications with their real gray level values.

For quantifying the texture using the SGLDM, 13 features are calculated. These features are calculated from the co-occurrence matrix, which is an estimate of the second order probability function $C(i,j|\Delta_x,\Delta_y)$. This matrix represents the probability of occurring a pixel pair with gray levels *i* and *j* given the distances between the pixels coordinates are Δ_x and Δ_y in the *x* and *y* directions, respectively. The elements of the matrix are calculated as follows:

$$C(i,\, j \mid \Delta_x, \Delta_y) = \frac{No.\ of\ \ (x,y)\ \ for\ \ which\ \ \ I(x,y)=i,\ I(x+\Delta_x, y+\Delta_x)=\ j\ and\ both (x,y)\ \ and\ \ (x+\Delta_x, y+\Delta_y)\ \ are\ \ within\ \ the\ \ ROI}{No.\ of\ (x,y)\ \ for\ \ which\ \ both\ (x,y)\ \ and\ (x+\Delta_x, y+\Delta_y)\ are\ within\ \ the\ \ ROI} \tag{7}$$

Sizes of the clusters range from 32 to 512 pixels. This causes some of the features in different images to be incomparable. In order to bring them to the same range, we divide the co-occurrence matrix by the area of the corresponding image. We calculate the co-occurrence matrices for 4 offset distances and 4 directions, i.e., we place the values of 1, 2, 3 and 4 in Δ_x and Δ_y, and the four angles 0^o, 45^o, 90^o and 135^o are defined for calculating the matrix for each of the 4 distances. This makes 16 matrices for each cluster. We calculate the 13 SGLDM features for each of these matrices. These features are named as follows: *angular second moment, contrast, correlation, variance, inverse difference moment, sum average, sum variance, sum entropy, entropy, difference variance, difference entropy*, and *two information measures of correlation*. Due to

the small number of pixels in the segmented images and infeasibility of calculating some of the features, we calculate only 9 features for each co-occurrence matrix when using the segmented microcalcifications.

The next step is to incorporate the features obtained for different directions (angles 0, 45, 90, 135) into one summary feature for each offset distance. This is accomplished because different directions should be treated the same for microcalcification feature extraction. For deriving these summary features, there are two possibilities: averaging the co-occurrence matrices over the angles and then calculating the features for each distance; or calculating the features for each of the four angles and then averaging the results. We have done both methods.

The second approach, as mentioned earlier, measures the texture of the clusters considering the calcifications and their background. Eleven Haralick features are included in these calculations. As a result, in the first approach 36 features, and in the second approach 44 features are obtained for each cluster.

3. FEATURE SELECTION

For selecting the best set of features, we use a GA-based global search method. The algorithm is based on Darwin's fittest principle, which states that an initial population of individuals evolves through natural selection in such a way that the fittest individuals have a higher chance of survival.[18] Seidlecki and Skalanski proposed a genetic algorithm for feature selection.[19] They encoded each individual as a binary string called chromosome with as many binary-coded genes as the feature space dimensionality. For evaluating the individuals, the features that correspond to a 1 in the chromosome are selected and used for classification. Then, a fitness value is assigned based on a performance measure in classification, e.g., the classification error. In another approach, a weight is assigned to each gene in the chromosome. Each weight is interpreted as the significance of its corresponding feature for classification. This means that before classification, each feature is multiplied by its weight. The weights are confined in a pre-defined interval. During evolution, the weights of the more relevant features tend to approach the maximum weight. The reverse is true for the less important features that act more like noise and convey small amounts of discriminative information for classification. By multiplying the features with an optimal set of weights, we actually modify the feature space in such a way that in the modified space, the distances between different classes are maximized. We have used both approaches in this paper.

Since the search space in a real-valued GA is much larger than that of binary-valued GA, we use a population large enough to cover the search space with a reasonable resolution. The large population size imposes a very high amount of computation. This is mainly due to the function evaluation stage that requires a complete classification process. To prevent the algorithm from becoming very slow and to benefit from a large population size at the same time, we use the following strategy. We divide the large-size population into several small-size subpopulations such that the computational burden is acceptable in each single subpopulation. In each generation, we consider a single population. Mating two best parents selected among the remaining subpopulations in subsequent iterations, we obtain as many offspring as the size of the subpopulation. In the next generation, the same steps are taken for the next subpopulation. This approach has two interesting features. First, we have many individuals in each generation where among them we can select the best ones. We thus obtain the variety in individuals, desirable in real-valued GA. Secondly, the speed of convergence will be manageable due to the fact that we only need to work with a single subpopulation in each generation. In this paper, we use 10 subpopulations each with a size of 100. This results in a total of 1000 individuals.

The parameters of real-valued GA are given in Table II. The two-point cross over operation chooses two uniformly random positions across the parents' chromosomes and then interchanges the sections to form the chromosome of the new offspring. We use boundary mutation in which a genotype is replaced with either the maximum or minimum weight value. In this study, we confine the weight of the features to be in the [0, 10] interval. In the binary GA case, the weights are chosen to be either 0 or 1.

One of the important parts in GA is selecting a proper criterion to be optimized. In this study, we use the area under the ROC curve, which we maximize. ROC analysis has been developed in the context of electronic signal detection and has been extensively applied to diagnostic systems in clinical medicine.[20] The ROC curve represents the false positive and true positive fractions for all the decision criteria the system might have. Decision criterion can be interpreted as a threshold above which a test is positive and below which it is negative. Since we use a kNN classifier, the decision criterion we choose is a measure of malignancy. We define the malignancy of a given sample to be the number of malignant neighbors among its k nearest neighbors. It thus ranges from 0 to k. To estimate malignancy of the samples, we change the threshold from –1 to k. When the threshold is set to be k, we announce all the samples as benign since the malignancy of none of the samples can exceed k. This causes both TPF and FPF to be 0. At the other extreme, TPF and FPF will be 1, when we choose threshold to

be -1. The rest of the points are obtained by changing the threshold between k-1 and 0. This will finally result in k+2 points of the ROC curve.

Table II. Parameters of GA used in this study.

Cross-over operation	Mutation operation	Cross-over probability	Mutation probability	Max. generation count
Two point cross-over	Boundary mutation	0.90	0.03	150

The area under the ROC curve is a number between 0 and 1. The area of 0.5 is no better than random classification. The more it approaches 1 the better the classification is. For computing the area under the ROC curve, we apply trapezoid rule to the curve points. Letting GA to go through its generations, we reach to a population in which the individuals yield a high value for the area under the ROC curve on average. Since ROC curve is an increasing curve, a near-one value of this area corresponds to a test for which a high value of true-positive fraction and a low value of false-positive fraction is expected for an appropriate threshold. This characteristic is most desirable in diagnostic tests.

4. EXPERIMENTAL RESULTS

4.1. Mammogram Database

We use the mammogram database developed by N. Karssemeijer in the University Hospital Nijmegen, the Netherlands.[21,22] The mammograms are recorded with a Kodak MIN-R/SO 177 screen/film combination. An Ekonix 1412 CCD camera was used to digitize the images. The spatial resolution was set to be 2048 by 2048 pixels per image with a gray level resolution of 12 bits per pixel. There are 40 mammograms in the database taken from 21 different patients. Both craniocaudal and oblique views are present for several of the patients. Each image contains one or more clusters of microcalcifications verified by histology and expert radiologists. A ground truth file accompanies each image, which has information about the location of the microcalcification cluster(s) in the image. The center coordinate and radius of the circle enclosing the cluster give this location. This area accounts for the Area Of Interest (AOI) that radiologist is assumed to mark on the mammogram before the Computer Aided Diagnostic (CAD) system begins its work. There are a total of 103 microcalcification clusters, 29 benign and 74 malignant cases, in the database with varying sizes and visibility. Containing microcalcification clusters with different visibility, this database is a good representative of clinical cases. Using look-up tables distributed along with the database,[22] we first noise-equalize the images.

4.2. Results

We have applied our feature selection procedure to the two sets of features described in Section 2. This procedure has been executed for 3 values of k in the kNN classifier algorithm. For each set of features, both the binary and the real-valued GA based feature selection methods have been applied. The results of using the feature selection algorithm are shown in Tables III and IV. The number of features are 17 for the shape features and 44 for the Haralick features. The second number in each cell of the tables shows how many features have taken part in the classification process. The fitted ROC curves using an exponential model are presented in Figures 2 and 3. Slight mismatch between numerical values in the tables and these figures are due to the fitting process.

Table III shows that the largest area under the ROC curve is 0.82 for k = 7. For this value of k only seven features took part in the classification process, which were the features 1, 2, 3, 5, 7, 13 and 14 in Table I. Features 1, 2, 5 and 14 also took part in the classification processes for other values of k. This shows their importance for discriminating between the benign and malignant microcalcification clusters.

Table IV shows the results for the Haralick features, obtained from the original (un-segmented) clusters. We had also extracted the same features for the segmented microcalcifications, but the results showed that these features are not able to classify the microcalcification clusters as good as the above-mentioned features. This may suggest that there is valuable texture information concerning the benignity or malignancy of the cluster in those areas of the images that lie outside the microcalcifications. The results show that the shape features outperform the Haralick features.

Table III. Area under the ROC curve and the number of features involved in classification, for three values of k for the 17 shape features, using the binary and real valued GA feature selection methods.

	k = 7	k = 9	k = 11
Results using binary GA	0.82 / 7	0.80 / 8	0.81 / 6
Results using real valued GA	0.78 / 14	0.79 / 11	0.79 / 14

Table IV. Area under the ROC curve and the number of features involved in classification, for three values of k for the 44 Haralick features, using the binary and real valued GA feature selection methods.

	k = 7	k = 9	k = 11
Results using binary GA	0.70 /4	0.72 / 4	0.71 / 2
Results using real valued GA	0.69 / 19	0.71 / 11	0.68 / 17

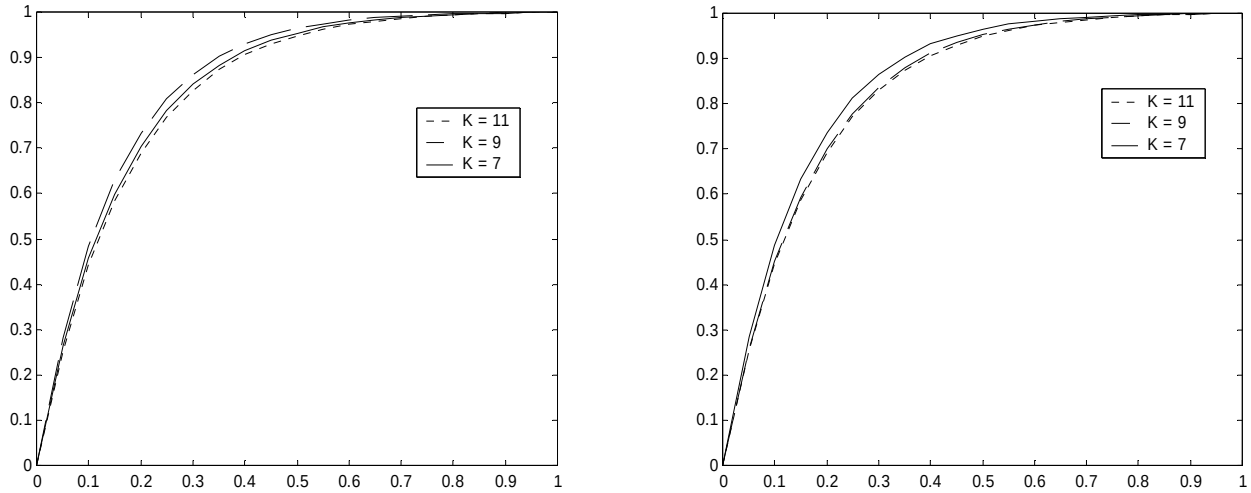

(a) (b)

Fig. 2. ROC curves (fitted to an exponential model) for the shape features for three values of k for (a) binary GA and (b) real-valued GA.

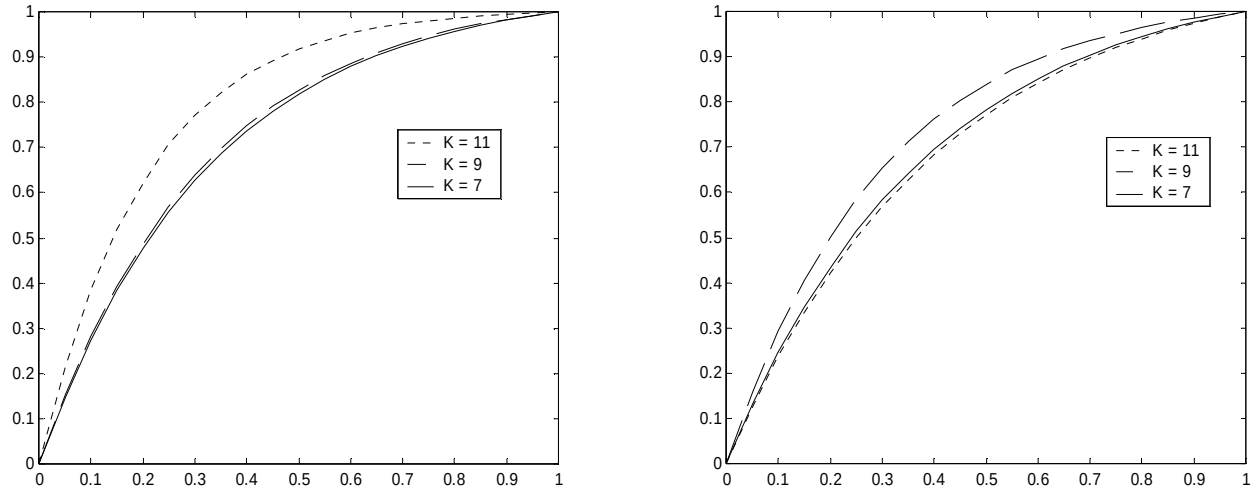

(a) (b)

Fig. 3. ROC curves (fitted to an exponential model) for the Haralick features for three values of k for (a) binary GA and (b) real-valued GA.

5. CONCLUSIONS

We compared the results of using two sets of features for classification of microcalcification clusters in mammograms. These two sets were based on shapes and textures of microcalcifications. The results show that the Haralick features extracted from the unsegmented clusters are able to classify the clusters into benign and malignant better than features extracted from the segmented clusters. This indicates that there is valuable information concerning the malignancy and benignity of these clusters in the texture surrounding the microcalcifications. Comparing the results obtained from applying the feature selection program to the two sets of features, it becomes clear that the shape features considerabily outperform the Haralick features. The important shape features that have resulted in the largest area under the ROC curve are the number of microcalcifications, the maximum size of them, the standard deviation of their size in the cluster, sum of the areas of calcifications in the cluster, average compactness, scattering of microcalcifications and average gray level of microcalcifications in the cluster. Comparing these to the main features that radiologists consider for classifying microcalcifcation clusters (number, shape, size, position and scattering of microcalcifications), we may conclude that using the same features for a CAD system is most appropriate. Incorporating other features such as texture features with these is expected to increase the power of the system to discriminate between the benign and malignant microcalcification clusters.

Comparing the results obtained for the two sets of features in the binary and real-valued GA cases, it is seen that they result in similar areas under the ROC curves while the binary method uses smaller numbers of features. In addition, the binary method is faster. Therefore, we may conclude that for this application this method is more appropriate.

ACKNOWLEDGMENT

This work was supported in part by the School of Intelligent Systems, Institute for Studies in Physics and Mathematics, Tehran, Iran.

REFERENCES

1. A. G. Haus, and M. J. Yaffe, “A categorical course in physics, Technical aspects of breast imaging,”in *Radiological society of North America*, 1993. Presented at the 79th scientific assembly and annual meeting.
2. Y. Jiang, RM. Nishikawa, DE. Wolverton, CE. Metz, RA. Schmidt, K. Doi, “Computerized classification of malignant and benign clustered microcalcifications in mammograms,” *Proc. of the 19th Annual Int. Conf. of the IEEE Eng. in Med. and Biol. Soc*., IEEE Part vol. 2, pp.521-3, 1997.
3. Y. Jiang, RM. Nishikawa, J. Papaioannou, “Requirement of microcalcification detection for computerized classification of malignant and benign clustered microcalcifications,” *Proc.* SPIE - the International Society for Optical Engineering, vol. 3338, pt. 1-2, pp. 313-17, 1998.
4. D. Betal, N. Roberts, GH. Whitehouse, “Segmentation and numerical analysis of microcalcifications on mammograms using mathematical morphology,” *British Journal of Radiology*, vol. 70, no. 837, pp. 903-17, 1997.
5. O. Tsujii, MT. Freedman, SK. Mun, “Classification of microcalcifications in digital mammograms using trend-oriented radial basis function neural network,” *Pattern Recognition*, vol. 32, no. 5, pp. 891-903, 1999.
6. W. Qian, LP. Clarke, D. Song, RA. Clark, “Digital mammography: hybrid four-channel wavelet transform for microcalcification segmentation,” *Academic Radiology*, vol. 5, no. 5, pp. 354-64, 1998.
7. Yu. Songyang, G. Ling, S. Brown, “Automatic detection of clustered microcalcifications in digitized mammogram films,” *Journal of Electronic Imaging*, vol. 8, no. 1, pp. 76-82, 1999.
8. Y. Songyang, G. Ling, “A CAD system for the automatic detection of clustered microcalcifications in digitized mammogram films,” *IEEE Trans. on Med. Imag*., vol. 19, no. 2, pp. 115-26, 2000.
9. MA. Gavrielides, JY. Lo, R. Vargas-Voracek, CE Jr. Floyd, “Segmentation of suspicious clustered microcalcifications in mammograms,” *Med. Phys.* , vol. 27, no. 1, pp. 13-22, 2000.
10. A.P. Dhawan, Y. Chitre, C. Kaiser-Bonaso, and M. Moskowitz, “Analysis of mammographic microcalcification using gray- level image structure features,” *IEEE Trans. Med. Imag*., Vol. 15, No. 3, June 1996.
11. I.E. Magnin, F. Cluzeuau, and C. L. Odet, “Mammographic texture analysis: An evaluation of risk for developing breast cancer,” *Opt. Eng*., Vol. 25, No. 6, pp. 780-784, 1986.
12. L. Shen, R. M. Rangayyan, and J. E. L. Desautels, “Application of shape analysis to mammographic calcifications,” in *IEEE Trans. Med. Imag*., vol. 13, no. 2, pp. 263-274, 1994.
13. F. Rafiee-Rad, H. Soltanian-Zadeh, M. Rahmati, S. Pour-Abdollah, “Microcalcification classification in mammograms using multiwavelet features,” *Proc. SPIE*, vol. 3813, pp. 832-41, 1999.
14. C. Heang-Ping, B. Sahiner, N. Petrick, MA. Helvie, L. Kwok Leung, DD. Adler, MM. Goodsitt, “Computerized classification of malignant and benign microcalcifications on mammograms: texture analysis using an artificial neural network,” *Phys. in Med. and Biol*., vol. 42, no. 3, pp. 549-67, 1997.

15. HP. Chan, B. Sahiner, KL. Lam, N. Petrick, MA. Helvie, MM. Goodsitt, DD. Adler, "Computerized analysis of mammographic microcalcifications in morphological and texture feature spaces," *Med. Phys*., vol. 25, no. 10. pp. 2007-19, 1998.
16. AP. Dhawan, Y. Chitre, C. Kaiser-Bonasso, "Analysis of mammographic microcalcifications using gray-level image structure features," *IEEE Trans. on Med. Imag*., vol. 15, no. 3, pp. 246-59, 1996.
17. P.A Freebrough., N.C. Fox, "MR Image Analysis Applied to the Diagnosis and Tracking of Alzheimer Disease," *IEEE Trans. Med. Imag.*, vol 17, no. 3, pp 475-479, 1998.
18. D. E. Goldberg, Genetic Algorithms in search, optimization and machine learning, Reading, MA: Addison-Wesley, 1989.
19. W. Siedlecki, and Skalanski, "On automatic feature selection," *Int. J. Pattern Recog. Art. Intell*., vol. 2, no., 2, pp. 197-220, 1988.
20. J. A. Swets, and R. P. Pickett, in evaluations of Diagnostic Systems: Methods From Signal Detection Theory, NewYork, Academic Press, 1982.
21. N. Karssemeijer, "A stochastic model for automated detection of calcifications in film mammograms," in *Proc. 12th Int. Conf. Inform. Processing Med. Imag*., Wye, UK, pp. 227-238, 1991
22. N. Karssemeijer, "Adaptive noise equalization and image analysis in mammography," in *13th Int. Conf. Inform. Processing and Med. Imag*., Flagstaff, AZ, 1992, pp. 427-486. (The Nijmegen database is available by anonymous FTP from figment.csee.usf.edu.)